

hep-ex/9703014

March, 1997

DEEP INELASTIC SCATTERING FROM UNPOLARISED TARGETS

G. K. MALLOT

*Institut für Kernphysik, Universität Mainz, Becherweg 45,
D-55099 Mainz, Germany*

In this paper the experimental status of unpolarised structure functions is reviewed. In particular the latest results from the NMC, E665, CCFR, and HERA experiments are discussed. Emphasis is put on the fixed-target experiments, which cover with high precision the x region relevant for the present polarised DIS experiments.

Invited Talk at the
International School of Nucleon Structure
1st Course: The Spin Structure of the Nucleon
Erice, Italy, 3–10 August 1995

DEEP INELASTIC SCATTERING FROM UNPOLARISED TARGETS

G. K. MALLOT

*Institut für Kernphysik, Universität Mainz, Becherweg 45,
D-55099 Mainz, Germany*

In this paper the experimental status of unpolarised structure functions is reviewed. In particular the latest results from the NMC, E665, CCFR, and HERA experiments are discussed. Emphasis is put on the fixed-target experiments, which cover with high precision the x region relevant for the present polarised DIS experiments.

1 Introduction

Deep inelastic scattering (DIS) of charged and neutral leptons has revealed most of what we know about the quark structure of the nucleon and of nuclei. The interpretation of DIS data is based on the factorisation of the hard scattering process from the nonperturbative nucleon structure. The former is described by Quantum Chromodynamics (QCD) while the latter is parametrised in terms of structure functions. Thus the objectives of DIS experiments are twofold. They test QCD and probe the nucleon's structure at the same time. DIS experiments led to the discovery of partons, which later were identified with the hypothetical quarks, postulated earlier to explain the hadron spectrum. It was also found that the charged partons are fermions with spin 1/2 and carry only about half of the nucleon's momentum. This suggests that gluons play an important rôle in the nucleon. The same partition was recently predicted for the angular momentum¹ in the limit of infinite momentum transfer, $Q^2 \rightarrow \infty$. With the advent of the high statistics experiments at large Q^2 , the gluon distribution could be inferred from the Q^2 dependence of the structure functions using the Gribov–Lipatov–Altarelli–Parisi evolution equations (GLAP).^{2,3,4} Important input for the flavour decomposition of the quark content of the nucleon came from charged-current neutrino scattering. It was shown that the nucleon contains three valence quarks and that the mean-square charge of the up and down quarks is 5/18. From opposite-sign di-muon events the distribution of the strange quarks was obtained.⁵

Although a consistent picture emerged and DIS developed to a precise tool, its history is accompanied by surprises. First strong effects due to nuclear binding⁶ were discovered by the European Muon Collaboration, the so-called EMC-Effect. Later the violation of the Ellis–Jaffe sum rule,⁷ discovered by the EMC^{8,9} in polarised muon-proton scattering, questioned our understanding of

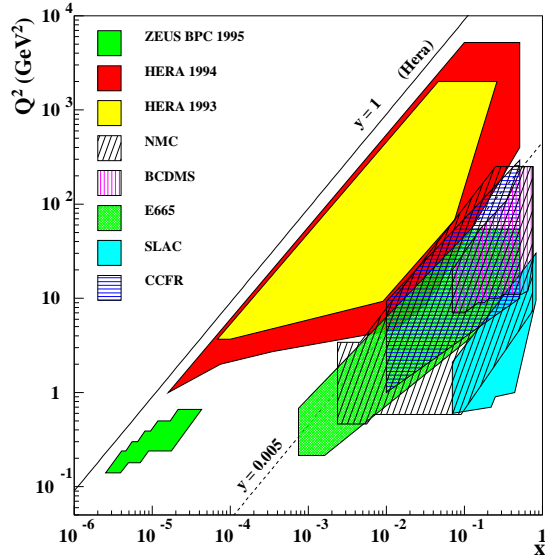
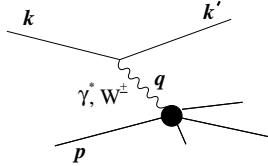


Figure 1: The deep inelastic scattering process. Figure 2: Kinematic range¹⁷ of the HERA, NMC, BCDMS, E665, SLAC, and CCFR experiments.

the nucleon's spin structure. Then the violation^{10,11} of the Gottfried sum rule¹² found by the New Muon Collaboration (NMC) revealed that the light quark sea is not flavour symmetric. Recently, a strong increase of F_2 at very small x was found at HERA^{13,14} and finally, the excess of events at high x and $Q^2 > 15000 \text{ GeV}^2$ also seen at HERA^{15,16} might be a trace of "new physics".

The DIS process is sketched in Fig. 1. The kinematics in the laboratory frame for fixed-target experiments is given by the incoming lepton energy, E , the energy transfer, $\nu = E - E'$, the square of the virtual-photon mass, $q^2 = -Q^2$, and the proton mass, M . In Born approximation the inclusive, differential cross section in terms of the scaling variables, $x = Q^2/2pq = Q^2/2M\nu$ and $y = pq/pk = \nu/E$, reads

$$\frac{d^2\sigma^{iN}}{dx dy} = a^{iN} \left\{ xy^2 F_1^{iN} + \left(1 - y - \frac{xyM^2}{s - M^2}\right) F_2^{iN} \pm \left(y - \frac{y^2}{2}\right) x F_3^{iN} \right\}, \quad (1)$$

where $F(x, Q^2)$ are the dimensionless structure functions and $s = Q^2/xy + M^2$ is the square of the lepton-nucleon c.m. energy. The coupling constants and

the boson propagators yield,

$$a^{\ell N} = 4\pi\alpha^2(s - M^2)\frac{1}{Q^4} \quad \text{and} \quad a^{\nu N} = \frac{G_F^2}{2\pi}(s - M^2)\frac{1}{(1 + Q^2/M_W^2)^2}, \quad (2)$$

for charged-lepton ($i = \ell$) and charged-current neutrino scattering ($i = \nu, \bar{\nu}$), respectively. The parity-violating structure function F_3 enters with positive (negative) sign for (anti)neutrino scattering and vanishes for electron and muon scattering. Neutral-current neutrino scattering and charged-current electron (muon) scattering^{18,19} are not discussed in this paper.

In the Quark-Parton-Model (QPM), which is motivated in the Bjorken limit, $Q^2, \nu \rightarrow \infty$ at fixed x , the scaling variable x represents the fraction of the nucleon's longitudinal momentum carried by the struck quark. The structure functions become functions of x only and acquire a very intuitive interpretation in terms of quark and antiquark distribution functions, $q_f(x)$ and $\bar{q}_f(x)$ with $q_f = u, d, s, c, b, t$. One finds the Callan-Gross relation,²⁰ $2xF_1(x) = F_2(x)$, and

$$\begin{aligned} F_2^{\ell N}(x) &= x \sum_f e_f^2 \{q_f(x) + \bar{q}_f(x)\}, \\ F_2^{\nu N}(x) = F_2^{\bar{\nu} N}(x) &= x \sum_f \{q_f(x) + \bar{q}_f(x)\}, \\ \frac{1}{2}x [F_3^{\nu N}(x) + F_3^{\bar{\nu} N}(x)] &= x \sum_f \{q_f(x) - \bar{q}_f(x)\}, \end{aligned} \quad (3)$$

where e_f denotes the electric charge of a quark with flavour f . In Eq. 3 neutrino scattering from isoscalar targets is assumed and in addition $s(x) = \bar{s}(x)$ and $c(x) = \bar{c}(x)$ is used in the expressions for $F_2^{\nu N}$ and $F_2^{\bar{\nu} N}$. In the QCD-improved QPM a logarithmic Q^2 dependence of the structure functions is generated by gluon bremsstrahlung. This Q^2 dependence can be calculated in QCD and is described by the GLAP equations. It is one of the cleanest tools to determine the gluon distribution function of the nucleon, $g(x, Q^2)$, and the strong coupling constant α_s .

In this paper emphasis is put on the results relevant to the analysis of the polarised DIS data, i.e. the region $0.001 < x$ and the main part of the paper is dedicated to fixed-target experiments. However, the most important results from HERA are also reviewed. The results from the Zeus experiment at HERA are discussed in more detail in a separate contribution²¹ to this Workshop. Due to the lack of space a discussion of nuclear effects in structure functions has been omitted.

2 The Experiments

The series of *unpolarised* electron DIS experiments at SLAC began in the late 1960's²² and lasted till 1985²³ and beyond. The scattered electrons were detected by 1.6, 8, and 20 GeV/ c small-aperture magnetic spectrometers. The maximum incident electron energy was 20 GeV covering the kinematic range $x \geq 0.07$.

In the 1980's the high-intensity 280 GeV CERN muon beam served simultaneously the experiment of the BCDMS and that of the European Muon Collaboration (EMC).²⁴ The momentum of the incident muon was measured by a dedicated common magnetic spectrometer. The EMC apparatus comprised an extended target area with an about 5 m long liquid hydrogen or deuterium target, a large-aperture spectrometer magnet and a muon-identification stage downstream of a hadron absorber. Subsequently upgraded versions of this spectrometer²⁵ were used by the New Muon (NMC) and by the Spin Muon Collaboration (SMC). The NMC experiments were optimised for the determination of cross-section ratios. A group of two targets along the beam axis was frequently exchanged with a second group of targets, in which the order of the target materials along the beam was inverted. This yielded very precise results for F_2^n/F_2^p ²⁶ and for nuclear effects in the structure functions.^{27,28} The BCDMS experiment consisted of a series of segmented toroids interspersed with MWPCs and trigger hodoscopes. The central bore contained the in total 40 m long targets. The muons were bent by the magnetic field in the iron toroids towards the axis of the spectrometer. This setup resulted in a good acceptance for large scattering angles, i.e. for large values of x and Q^2 . The to date last unpolarised muon DIS experiment was performed by the E665 Collaboration²⁹ using the 470 GeV muon beam at FNAL. The principle of the spectrometer is similar to that of the EMC. However, it involved an additional spectrometer magnet close to the target.

In the early 1980's also charged-current neutrino–nucleon scattering experiments started at CERN with the CDHSW experiment.³⁰ The most precise data today come from the CCFR Collaboration at FNAL, which took data in the late 1980's. Neutrinos and antineutrinos of 30–600 GeV from kaon and pion decays impinged on a 690 ton iron target and the emerging muons were detected in a 420 ton toroid system. Apart from $F_2^{\nu N}$ and $F_3^{\nu N}$ results for the Gross-Llewellyn Smith sum rule³¹ and the strange quark content of the nucleon⁵ were obtained.

Finally, in the 1990's the HERA e-p collider at DESY with its H1 and ZEUS²¹ experiments opened up a completely new kinematic domain. The 820 GeV proton and the 27 GeV electron beam provide a centre-of-mass energy

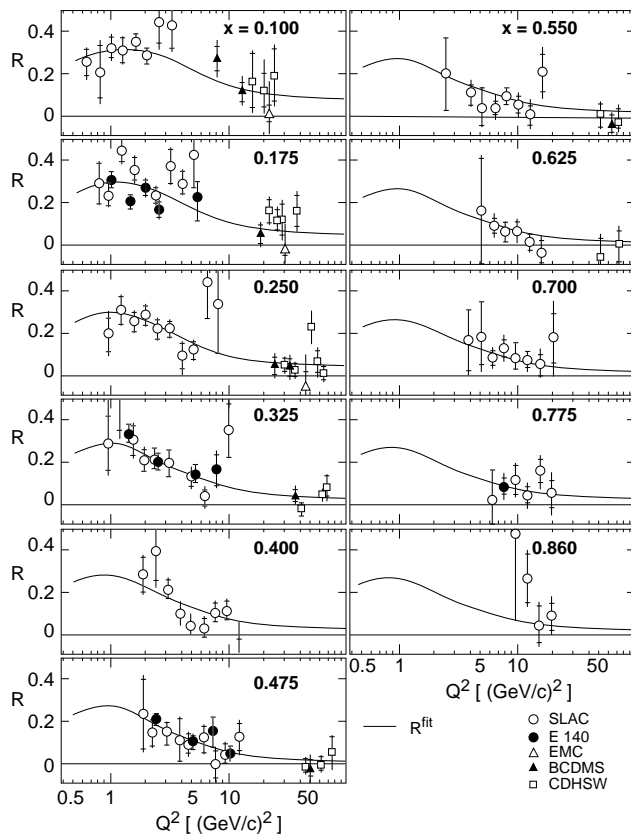


Figure 3: SLAC analysis of $R(x, Q^2)$ data.³² The solid curve is a parametrisation of the data, which is widely used (R1990).

of $\sqrt{s} \simeq 300$ GeV with which x values as low as $x = 10^{-4}$ can be reached at a momentum transfer of $Q^2 \simeq 5$ GeV² and for $x > 0.1$ values of $Q^2 \geq 5000$ GeV² can be accessed. The kinematic range of the individual experiments is shown in Fig. 2.

3 The Longitudinal-to-Transverse Cross-Section Ratio

Both, longitudinally and transversely polarised photons contribute to the differential cross section of Eq. 1. The ratio of the corresponding cross sections,

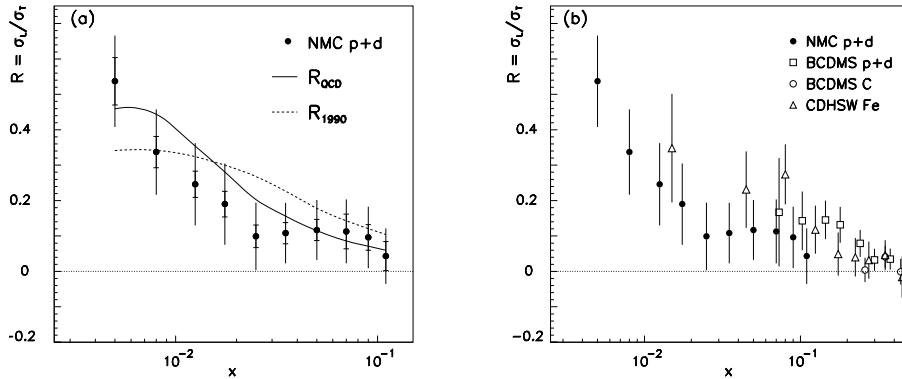


Figure 4: (a) NMC measurement³⁴ of R as function of x together with the R1990 (solid line) parametrisation³² and R_{QCD} (dashed line). (b) Comparison with several other experimental results.

σ_L and σ_T , is given by

$$R = \frac{\sigma_L}{\sigma_T} = \frac{F_2(1 + Q^2/\nu^2)}{2xF_1} - 1 = \frac{F_L}{2xF_1}. \quad (4)$$

It can be determined from measurements at the same (x, Q^2) point at different values of y , i.e. different incident lepton energies. Transverse quark momenta introduced by gluon bremsstrahlung allow also the absorption of longitudinal virtual photons. Due to the absence of transverse momenta, F_L vanishes in the naïve QPM. In perturbative QCD F_L and thus R (R_{QCD}) can be calculated³³ from F_2 and from the gluon distribution function, g ,

$$F_L(x, Q^2) = \frac{\alpha_s}{\pi} x^2 \left\{ \frac{4}{3} \int_x^1 F_2(y, Q^2) \frac{dy}{y^3} + 2c \int_x^1 g(y, Q^2) \left(1 - \frac{x}{y}\right) \frac{dy}{y^2} \right\}, \quad (5)$$

where $c = \sum e_f^2$ for electron and muon scattering and $c = n_f$, the number of active flavours, for neutrino scattering. Note that F_L is proportional to the strong coupling constant $\alpha_s(Q^2)$. At small values of x , where $g(x, Q^2)$ rises sharply, an increase of F_L is expected from Eq. 5.

The result of a comprehensive global analysis³² of the the SLAC electron-proton and deuteron data on $R(x, Q^2)$ and some high Q^2 muon and neutrino data from CERN resulted in a phenomenological parametrisation for R , often referred to as R1990, which is shown together with the data in Fig. 3. The kinematic region covered is $0.1 \leq x \leq 0.9$ and $0.6 < Q^2 < 20 \text{ GeV}^2$ for the SLAC data and up to about 80 GeV^2 for the muon and neutrino data. The ratio R is

rather well determined for intermediate x and large Q^2 , where it is small. However, the behaviour in the region $x < 0.1$ is uncertain. Recently, new data from the NMC³⁴ in the small- x region, $0.002 < x < 0.12$, became available (Fig. 4). The data agree well with the rise expected from perturbative QCD and – in the region of overlap – with the previous measurements. Also the preliminary neutrino data for R from the CCFR Collaboration³⁵ for $0.01 < x < 0.6$ and $Q^2 > 4 \text{ GeV}^2$ agree well with R_{QCD} (not shown here). The comparison of the neutrino R data taken with an iron target and the charged-lepton data shows no evidence for a dependence of R on the target material. Similar conclusions were previously reached from muon^{36,26} and electron experiments^{37,38,39} using a series of nuclear targets.

A measurement of F_L at very small x is presently being considered at HERA using lower beam energies. First results were obtained from the 1994 H1 data⁴⁰ using a different approach. Equation 1 can be rewritten in terms of F_2 and F_L yielding a differential cross section proportional to $(2 - 2y + y^2)F_2 - y^2F_L$. Thus at small y the cross section is dominated by F_2 , while F_2 and F_L contribute with similar weight at large y . The longitudinal structure function F_L was determined from the data with $0.6 \leq y \leq 0.78$ by subtracting the F_2 contribution, which was obtained from data with $y \leq 0.35$. Since both data sets were taken using same beam energies, the F_2 data had to be evolved from the measured Q^2 to the value corresponding to the higher value of y using next-to-leading order GLAP evolution. In this sense $F_L(x, Q^2)$ was not directly measured but inferred from data taken at different (x, Q^2) points. The result, $F_L = 0.52 \pm 0.25$ at $x = 0.00024$ and $Q^2 = 15.4 \text{ GeV}^2$, corresponds to $R \simeq 0.50$ and agrees well with expectations.

4 Structure Function Data

4.1 Muon and Electron Fixed-Target $F_2(x, Q^2)$ Data

The present status of the deuteron F_2 measurements from charged-lepton fixed-target experiments is summarised in Figs. 5 and 6. The proton data are in accuracy and kinematic coverage similar to the deuteron results. The data from SLAC,²³ the NMC,³⁴ and the BCDMS^{41,42} collaboration are in excellent agreement. They exhibit strong scaling violations, which are positive at small x and negative at large x . The EMC F_2 data^{43,44} deviate systematically⁴⁵ from the BCDMS and NMC data at small x . This discrepancy remained also after a re-analysis⁴⁶ of the EMC data, which therefore were not included in this compilation. At large x and Q^2 the data are dominated by the results from the BCDMS while the small x and Q^2 region is the domain of the SLAC

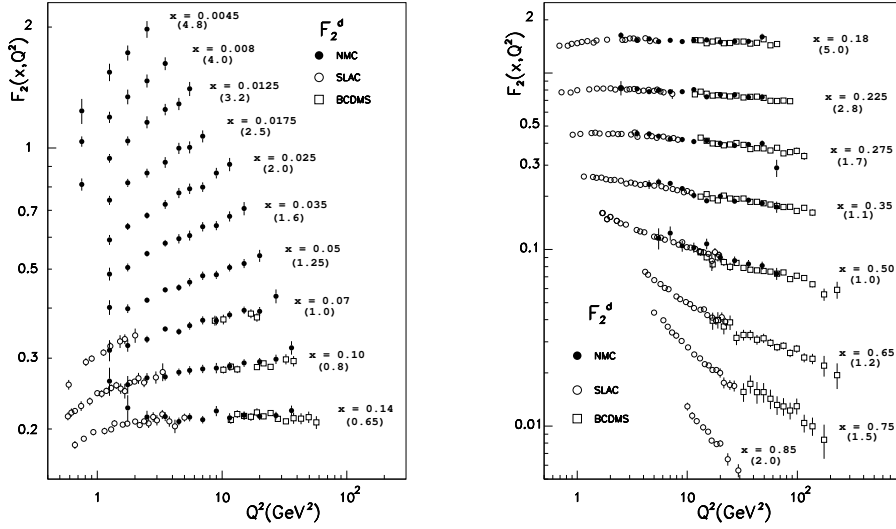


Figure 5: The structure function F_2 for the deuteron³⁴ from the SLAC, BCDMS, and NMC experiments. The data were multiplied with the numbers in brackets for clarity of the plot.

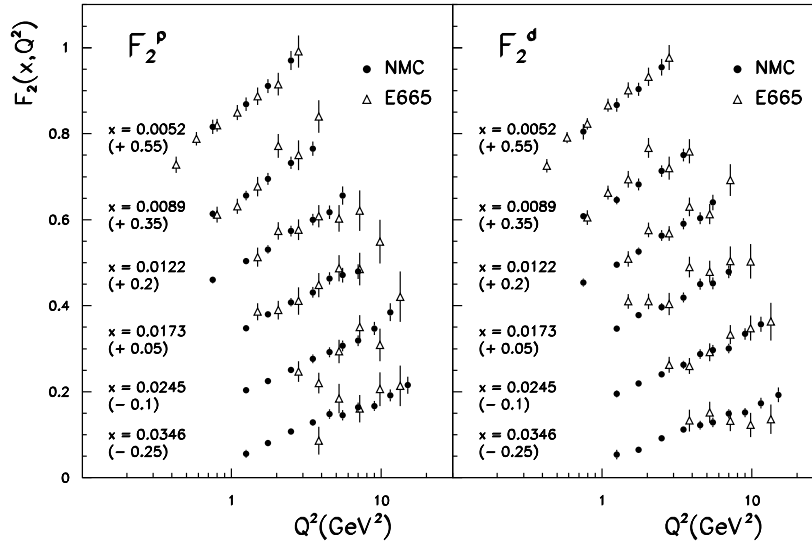


Figure 6: Comparison of the NMC³⁴ and E665²⁹ F_2 data for the proton (left) and the deuteron (right) in the range $0.004 < x < 0.04$. The values in the brackets were added to the data for clarity of the plot.

data. The final analysis of the NMC F_2 data comprises all the data taken with 90, 120, 200, and 280 GeV muon beams. The NMC data provide the link between the SLAC and BCDMS data and extend the measured x region by more than an order of magnitude from $x = 0.07$ down to $x = 0.0045$. A useful phenomenological parametrisation to the NMC, BCDMS, and SLAC data is given in Ref. [47]. A comparison of the NMC data with the E665 data²⁹ for the proton and the deuteron in the range $0.004 < x < 0.04$ is shown in Fig. 6. The E665 data extend over five more small- x bins not shown here down to $x = 0.0008$ where the average Q^2 is about 0.4 GeV^2 . A comparison of the HERA data from H1⁴⁸ and Zeus⁴⁹ to the NMC data, which are considerably more accurate, is shown in Fig. 7. The HERA data are in fair agreement with the extrapolation of the NMC data to larger values of Q^2 .

4.2 The ratio F_2^n/F_2^p and the Gottfried sum rule

Recent measurements of the structure function ratio F_2^n/F_2^p come from the NMC²⁶ and the E665 Collaboration⁵⁰ (Fig. 8). The neutron-to-proton structure function ratio is obtained from experiments with liquid hydrogen and deuterium targets. Neglecting nuclear effects in the deuteron the ratio is given by

$$\frac{F_2^n}{F_2^p} = 2 \frac{F_2^d}{F_2^p} - 1 = 2 \frac{\sigma^d}{\sigma^p} - 1. \quad (6)$$

The latter step in Eq. 6 is justified by several measurements^{32, 39, 26} finding the difference $R^d - R^p$ to be compatible with zero in the range $0.003 < x < 0.8$. This puts via Eq. 5 a limit²⁶ on a possible difference of the gluon distributions in the proton and the deuteron. The ratio F_2^n/F_2^p is found to be largely independent of Q^2 . Small negative Q^2 slopes, $d(F_2^n/F_2^p)/d \ln Q^2$, were observed²⁶ in the range $0.1 < x < 0.5$ in agreement with predictions from perturbative QCD. The ratio F_2^n/F_2^p approaches unity for $x \simeq 0.001$ as expected in this region where the sea quarks dominate. The small deviation from unity is in the order of 0.02, which is a typical value expected for shadowing corrections in the deuteron.^{51, 52} At very small x the E665 data indicate a drop below 0.9. Note however, that Q^2 is as small as 30 MeV^2 for $x = 6 \times 10^{-6}$, what makes the data difficult to interpret.

The NMC used the ratio F_2^n/F_2^p together with F_2^d to test the Gottfried sum rule¹²

$$S_G = \int_0^1 \frac{F_2^p - F_2^n}{x} dx = \frac{1}{3} + \frac{2}{3} \int_0^1 (\bar{u} - \bar{d}) dx. \quad (7)$$

If the last term vanishes the Gottfried sum rule takes its original form, $S_G = 1/3$. The NMC finds¹¹ $S_G = 0.235 \pm 0.026$ at $Q^2 = 4 \text{ GeV}^2$ significantly below

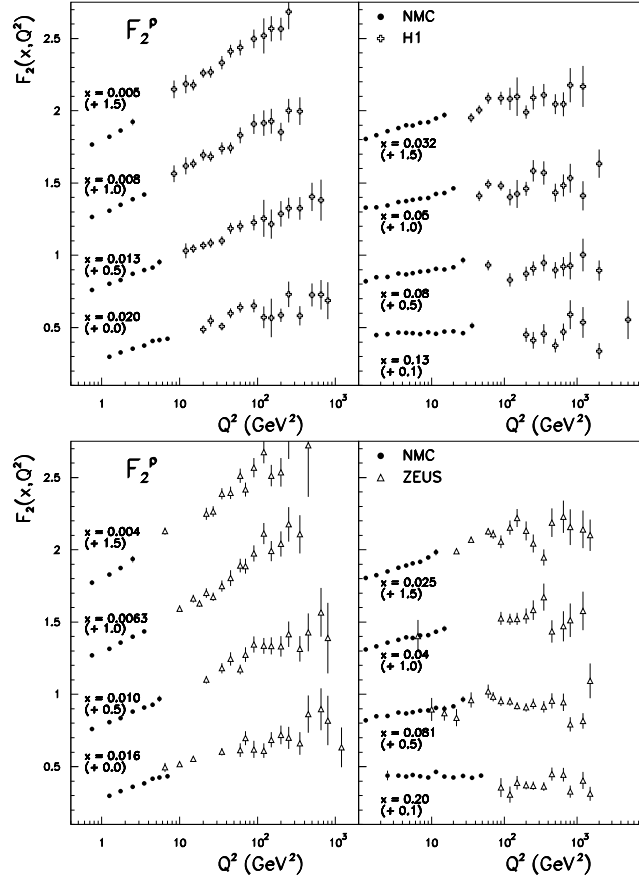


Figure 7: Comparison³⁴ of the NMC F_2^P data with the present HERA data from H1⁴⁸ (top) and ZEUS⁴⁹ (bottom) in the range $0.004 < x < 0.2$.

1/3. From Eq. 7 it is obvious that this result can be interpreted as a flavour-asymmetric sea yielding $\int_0^1 (\bar{u} - \bar{d}) dx = -0.165 \pm 0.059$. This explanation is supported by the CERN experiment NA51, in which the cross-section asymmetry $(\sigma^{PP} - \sigma^{Pn})/(\sigma^{PP} + \sigma^{Pn})$ for Drell-Yan production of muon pairs was measured using proton and deuteron targets. From the asymmetry a value of $\bar{u}(x)/\bar{d}(x) = 0.51 \pm 0.06$ at $x = 0.18$ was inferred.⁵³ Both, the NMC and NA51 experiment, find a larger down than up-quark component in the proton's quark sea.

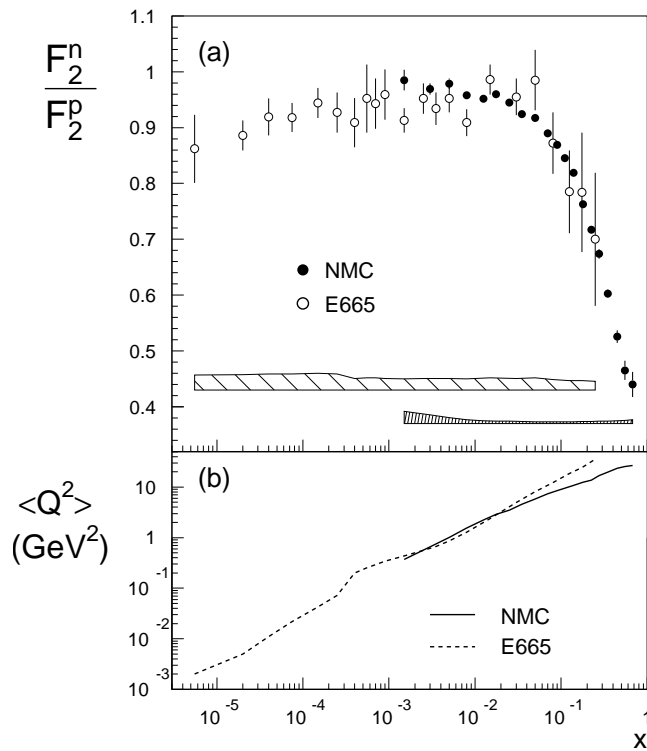


Figure 8: (a) The neutron-to-proton structure function ratio, F_2^n/F_2^p , as a function of x from the NMC²⁶ and E665.⁵⁰ The shaded bands indicate the size of the systematic uncertainties. (b) Average Q^2 of the NMC and E665 data as a function of x .

4.3 Data from Neutrino Experiments

The nucleon's structure functions, $F_2^N = (F_2^p + F_2^n)/2$, measured in charged-lepton and neutrino experiments are related by (see Eq. 3)

$$\frac{F_2^{\ell N}}{F_2^{\nu N}} = \langle e^2 \rangle \left\{ 1 - \frac{3}{5} \frac{(s + \bar{s}) - (c + \bar{c})}{\sum q + \bar{q}} \right\}, \quad (8)$$

where $\langle e^2 \rangle = (e_u^2 + e_d^2)/2 = 5/18$ is the mean square charge of the up and down quarks. An analysis⁵⁵ using the BCDMS and CCFR data yields $\langle e^2 \rangle = (1.00 \pm 0.03) \cdot 5/18$. Neutrino data are taken with heavy nuclear targets and must be corrected for both, nuclear effects and non-isoscalarity, before being compared to deuteron data from charged-lepton experiments. These correc-

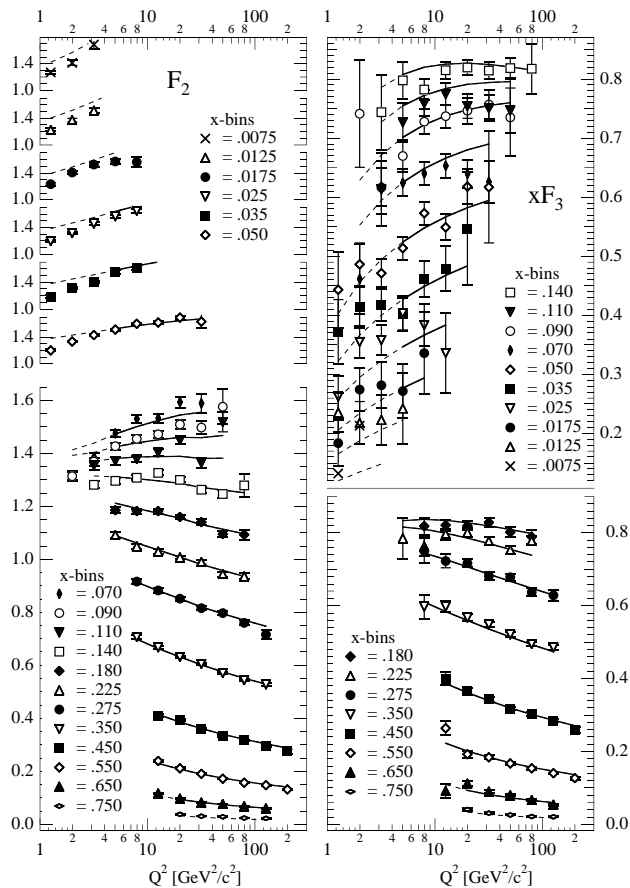


Figure 9: The CCFR F_2 and xF_3 structure functions as a function of Q^2 for different values of x .⁵⁴ Also shown is a QCD fit to the data (solid line) and its extrapolation to lower Q^2 (dashed line).

tions are assumed to be equal to those in charged-lepton scattering where they are well measured.^{56,27,57} In addition to F_2 the parity-violating, nonsinglet structure function xF_3 , which measures the difference of quark and antiquark contributions, can be studied in neutrino and antineutrino scattering.

The most precise data for deep-inelastic neutrino scattering come from the CCFR Collaboration at FNAL. The complete F_2 and xF_3 data sets are shown in Fig. 9. For $x \geq 0.1$ good agreement of the corrected CCFR iron F_2 data^{55,54}

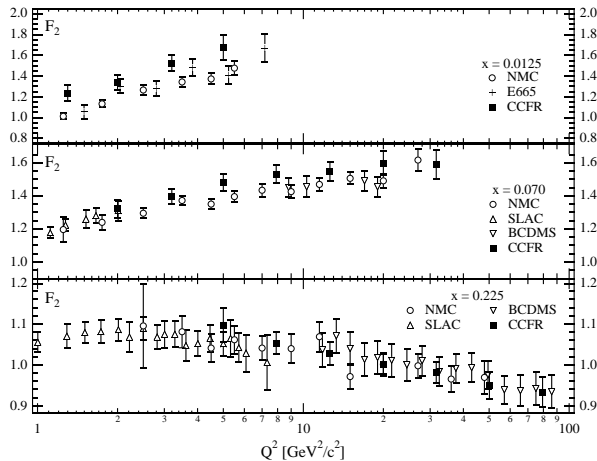


Figure 10: Comparison of the F_2 data from neutrino and charged-lepton scattering for the bins $x = 0.0125, 0.070,$ and 0.225 .⁵⁴

with the NMC and BCDMS deuteron data is found. However, in the small region, $x < 0.01$, the neutrino data are up to 20 % larger (Fig. 10). In the first x bins this discrepancy, which decreases systematically with increasing x , is outside the statistical and systematic errors. In this region the strange sea contribution may become important. The strange-quark content of the nucleon was determined directly⁵ from neutrino-induced charm production, $\nu_\mu s \rightarrow \mu^- c$, and analysed in terms of the parameter

$$\kappa = \frac{\int_0^1 x s(x) + x \bar{s}(x) dx}{\int_0^1 x \bar{u}(x) + x \bar{d}(x) dx}. \quad (9)$$

In a next-to-leading order analysis a value of $\kappa = 0.477 \pm 0.051$ was found establishing a suppression of the strange sea. The shape of the strange quark distribution function, $s(x)$, is compatible with that of the light antiquarks. A possible difference between the strange and antistrange distribution functions, $s(x) \neq \bar{s}(x)$, which is expected for an intrinsic strangeness component in the nucleon,^{58,59} is beyond the precision of the present data. A fit allowing different shapes for $s(x)$ and $\bar{s}(x)$, with $s(x)/\bar{s}(x) = A(1-x)^{\Delta\alpha}$, yielded $\Delta\alpha = -0.46 \pm 0.87$. The strangeness content found in this measurement is not sufficient to explain the discrepancy between the charged-lepton and neutrino F_2 data at $x \leq 0.1$. Possible other sources for the discrepancy are discussed in Refs. [60, 61, 62]

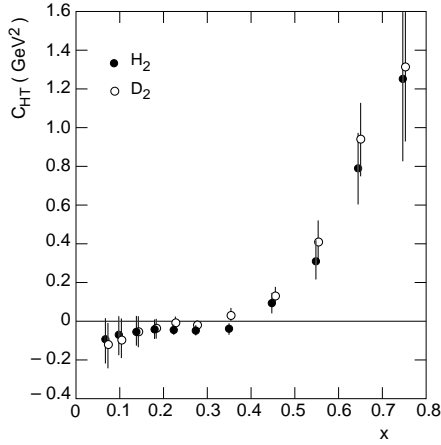


Figure 11: Higher-twist coefficients for the proton and the deuteron as a function of x .⁶³

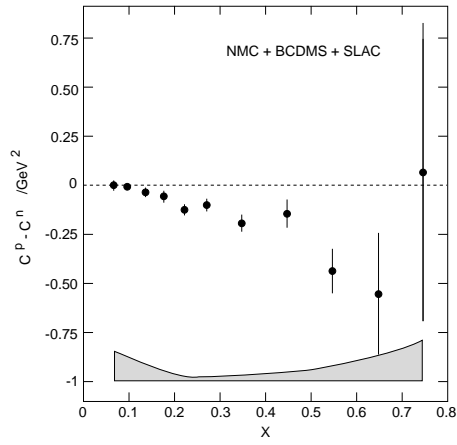


Figure 12: The difference of the higher twist coefficients of the proton and the deuteron as a function of x .⁶⁴

5 QCD analyses and determination of α_s

Perturbative QCD predicts the Q^2 evolution of the flavour singlet, $q^s(x, Q^2) = \sum_f q_f(x, Q^2)$, and nonsinglet, $q^{ns}(x, Q^2) = q_i(x, Q^2) - q_j(x, Q^2)$, quark distribution functions and of the gluon distribution function, $g(x, Q^2)$. The quark singlet combination evolves coupled to the gluons while quark nonsinglet combinations evolve independently. Typical nonsinglet combinations are the difference of quarks and antiquarks, xF_3 , and the difference of up and down quarks, $F_2^p - F_2^n$, while F_2^d is almost a pure singlet combination. Apart from a test of QCD the aim of QCD analyses of the structure function data is the determination of the parton distribution functions and of the strong coupling constant, α_s . The parton distribution functions are parametrised at a starting scale Q_0^2 and are then evolved to the Q^2 of the data points according to the GLAP equations.

For the BCDMS/SLAC,⁶³ the NMC,⁶⁵ and the CCFR⁵⁴ data next-to-leading order QCD analyses were carried out by the experimental groups. In the BCDMS and NMC analyses the proton and deuteron data were fitted simultaneously. The data included in the BCDMS fit cover $0.07 < x < 0.85$ with Q^2 in the range $0.5\text{--}260 \text{ GeV}^2$. In addition to the leading-twist contribution and target-mass corrections,⁶⁶ combined in F_2^{LT} , higher-twist corrections had

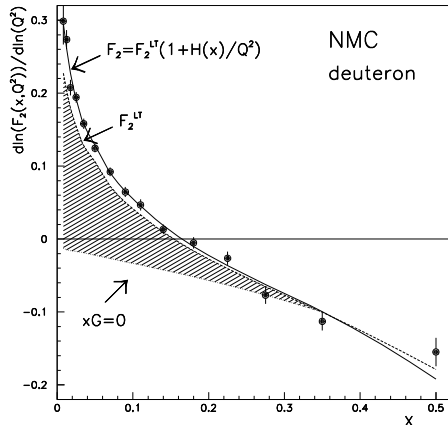


Figure 13: The logarithmic slopes $d \ln F_2 / d \ln Q^2$ of the NMC deuteron data as a function of x . The solid line shows the slopes obtained from the NLO QCD analysis.⁶⁵ The dashed line correspond the the QCD prediction without higher-twist terms and the dotted line to the Q^2 evolution due to quarks only.

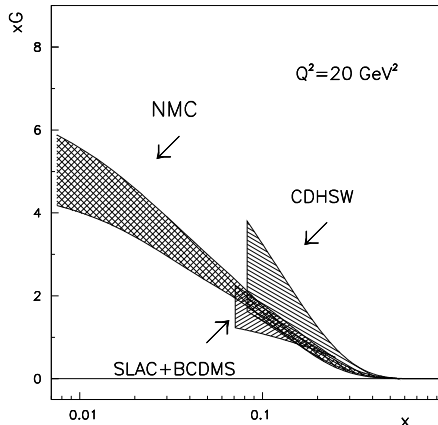


Figure 14: The gluon distribution function from the NMC QCD analysis⁶⁵ as function of x at 20 GeV^2 compared to that from the analysis of the BCDMS/SLAC data⁶³ and that of a LO analysis of CDHSW data.³⁰

to be included to describe the data. They were parametrised in the form

$$F_2(x_i, Q^2) = F_2^{LT}(x_i, Q^2) \left\{ 1 + \frac{c_i}{Q^2} \right\}, \quad (10)$$

where c_i is the higher-twist coefficient for the i th x bin. The fitted coefficients for the proton, c_i^p , and for the deuteron, c_i^d , are shown in Fig. 11. A calculation of these coefficients using infrared renormalons is in good agreement with the experimental results.⁶⁷ The differences of the proton and neutron coefficients, $c_i^p - c_i^n$ were studied with higher precision in a combined analysis⁶⁴ of F_2^n/F_2^p data from the NMC, BCDMS, and SLAC experiments (Fig. 12).

The higher-twist coefficients from the BCDMS analysis were used in the next-to-leading order QCD analysis⁶⁵ of the NMC data with $Q^2 > 1 \text{ GeV}^2$. This analysis was the first to focus on the small x region, $0.008 < x < 0.5$, where the gluon contribution dominates. This is demonstrated in Fig. 13, where the total QCD evolution and that due to quarks as obtained from the QCD fit is shown separately. At $x = 0.01$ the gluon distribution function was determined with a precision of 20 % (Fig. 14). The total momentum fraction

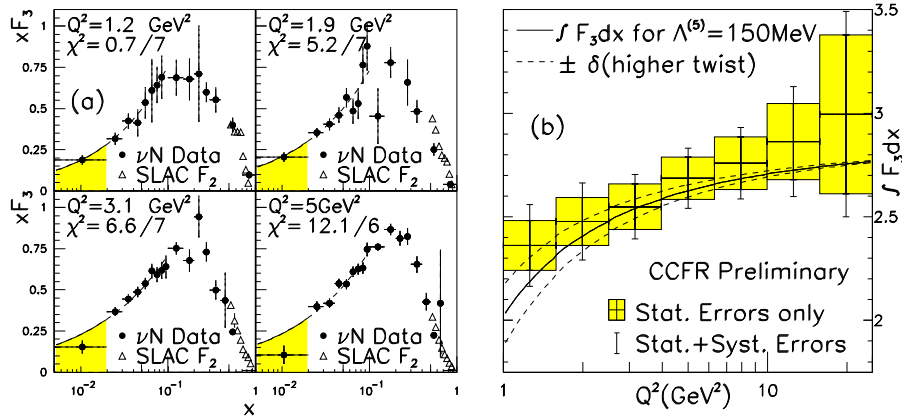


Figure 15: (a) The structure function $x F_3$ as function of x for four Q^2 bins. (b) GLS sum as function of Q^2 .⁶⁹

carried by quarks and gluons in the region covered by the data amounts to 0.95 and the quarks carry a momentum fraction of 0.55 ± 0.02 at $Q_0^2 = 7 \text{ GeV}^2$.

In the QCD analysis⁵⁴ of the CCFR F_2 and $x F_3$ structure functions, data with $Q^2 < 5 \text{ GeV}^2$ or a hadronic final-state energy of $W^2 < 10 \text{ GeV}^2$ were excluded. This largely removed the small- x region, where the charged-lepton and the neutrino F_2 data differ. The fit is shown as solid line in Fig. 9. The value obtained for the strong coupling constant, $\alpha_s(M_Z^2) = 0.119 \pm 0.004$, is considerably larger than the one found in a previous analysis⁶⁸ of the same data, $\alpha_s(M_Z^2) = 0.111 \pm 0.004$. The change by two standard deviations is mainly attributed to changes in the energy calibration. The results for $\alpha_s(M_Z^2)$ are summarised in Table 1 together with some typical parameters of the fits. The contributions from the different error sources were added in quadrature.

The Q^2 dependence of moments of structure functions is directly predicted by the operator-product expansion. The GLAP equations can be obtained by a transformation from moment to coordinate space. Therefore the study of moments of structure functions is particularly interesting from the theoretical point of view. However, the extrapolations to $x = 0$ (and $x = 1$) and the fact that the sum rules must be evaluated at a fixed value of Q^2 for all values of x introduces additional experimental uncertainties. The Gross–Llewellyn Smith sum rule⁷³ (GLS) for the parity-violating structure function $x F_3$ states that

Table 1: Results for α_s from NLO QCD analyses of DIS data

Data	Ref.	Q_{\min}^2	Q_0^2	$\alpha_s(M_Z^2)$
BCDMS/SLAC	63	0.5 GeV ²	20 GeV ²	0.113±0.005
NMC	65	1.0 GeV ²	7 GeV ²	0.117 $^{+0.011}_{-0.016}$
CCFR	54	5.0 GeV ²	5 GeV ²	0.119±0.004
HERA	70			0.120±0.010
CCFR (GLS,	71		3.0 GeV ²	0.115±0.006
NNLO)	69		1–20 GeV ²	0.108 $^{+0.007}_{-0.009}$
PDG	72			0.118±0.003

the nucleon contains three valence quarks

$$S_{GLS} = \frac{1}{2} \int_0^1 \frac{x F_3}{x} dx = 3 \left(1 - \frac{\alpha_s}{\pi} - \mathcal{O}(\alpha_s^2) \right). \quad (11)$$

The valence quarks represent a flavour-nonsinglet quark combination like the difference of up and down quark polarisations, $\Delta u - \Delta d$, in the famous Bjorken polarisation sum rule.⁷⁴ The QCD corrections for both sum rules are known to order $\mathcal{O}(\alpha_s^3)$.⁷⁵ The CCFR Collaboration has evaluated the GLS sum at $Q^2 = 3 \text{ GeV}^2$ as $S_{GLS} = 2.50 \pm 0.018(\text{stat.}) \pm 0.078(\text{syst.})$.³¹ This yields in next-to-next-to-leading order $\alpha_s(M_Z^2) = 0.115 \pm 0.006$.⁷¹ In this analysis the structure functions were evolved from the Q^2 of the measurement to 3 GeV² using the GLAP equations. To avoid any Q^2 evolution of the data a new analysis was performed⁶⁹ including data from other experiments. In particular, F_2 data from SLAC were used for $x > 0.5$, where the antiquark contribution becomes negligible and thus $x F_3 \simeq F_2$. The GLS sum was evaluated for seven Q^2 bins between 1 and 20 GeV² (Fig. 15). The data with $Q^2 < 7 \text{ GeV}^2$ average to $\alpha_s(M_Z^2) = 0.108^{+0.007}_{-0.009}$. This value differs considerably from the one found in the re-analysis of scaling violations in F_2 and $x F_3$ and from the present world average $\alpha_s(M_Z^2) = 0.118 \pm 0.003$.⁷²

6 HERA data for F_2^p

The HERA experiments H1 and ZEUS²¹ have extended the kinematic range of F_2^p measurements down to $x \simeq 10^{-5}$ and to $Q^2 > 5000 \text{ GeV}^2$ for $x > 0.1$. The HERA F_2 data^{48,49} taken in 1994 agree fairly with the high Q^2 extrapolation of the fixed-target data as shown in Figs. 16, 17, and 7. In the small- x region a steep rise of $F_2 \sim x^{-\lambda}$ is observed for decreasing x . The

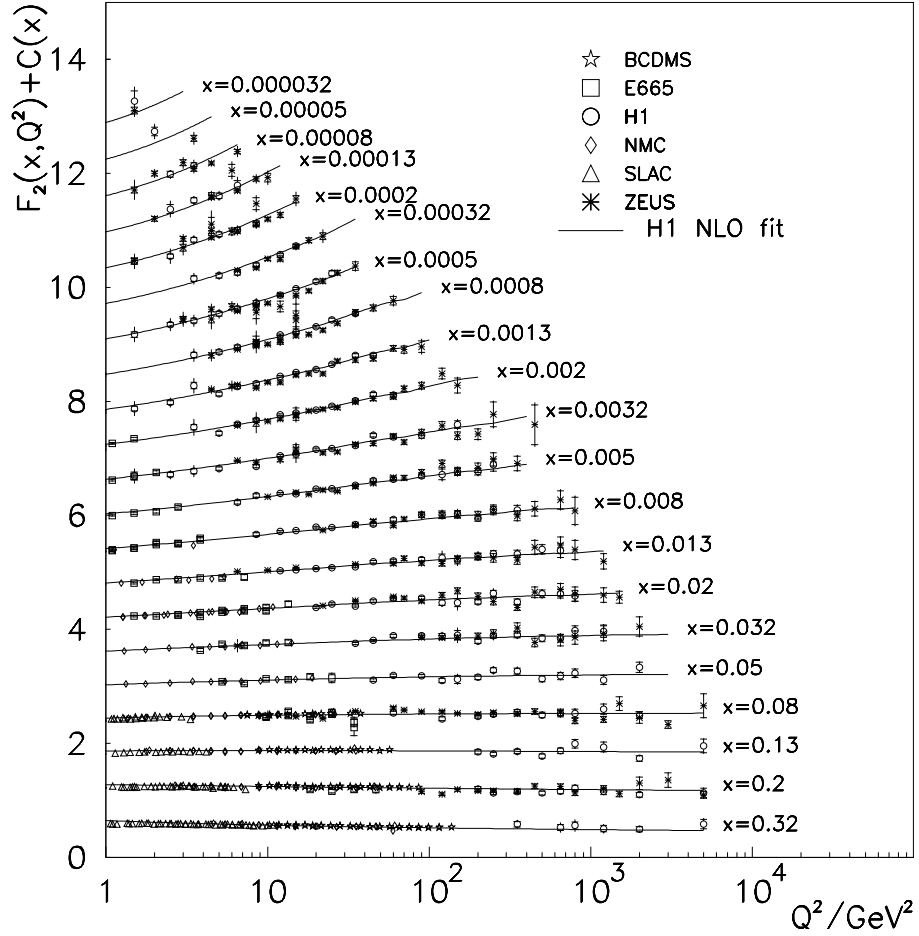


Figure 16: Hera F_2 data^{48,49} from the 1994 run as function of Q^2 for different values of x together with those from fixed-target experiments. Also shown is a NLO QCD fit⁴⁸ to the H1, NMC, and BCDMS data with $Q^2 > 5 \text{ GeV}^2$. The constants $C(x)$ are defined by $C(x) = 0.6(i - 0.4)$ with the x -bin number i and $i = 1$ for $x = 0.32$.

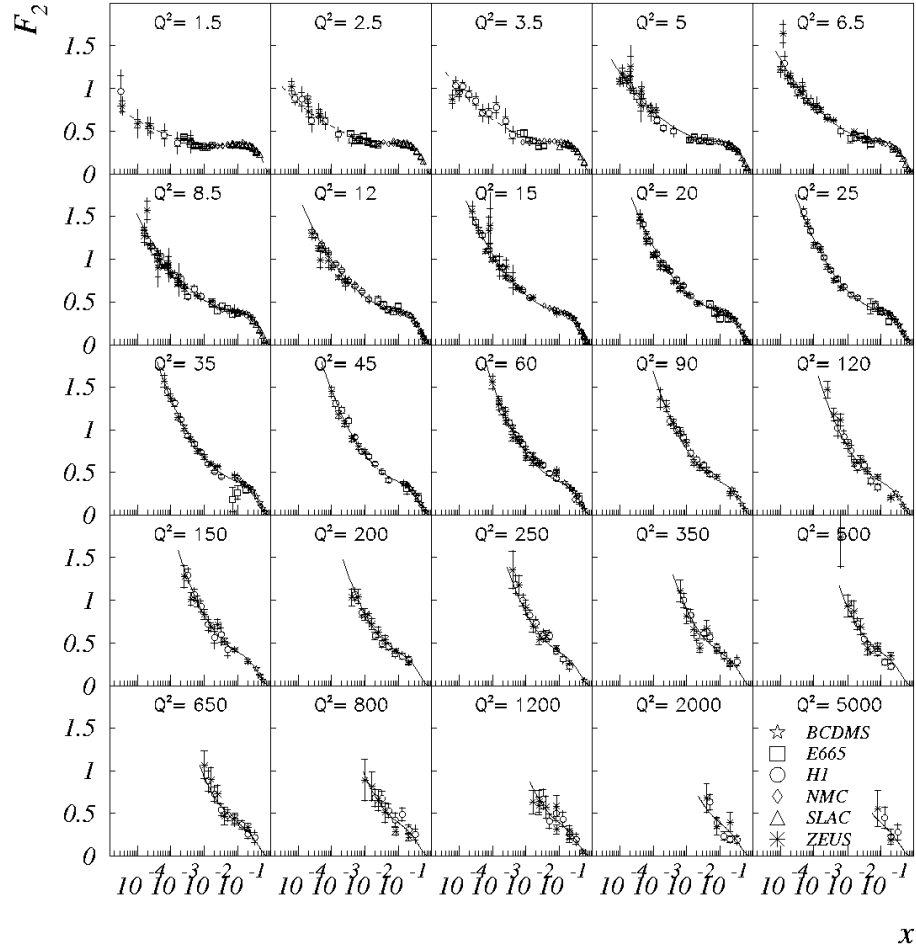


Figure 17: Hera F_2 data^{48,49} from the 1994 run as function of x for different values of Q^2 together with data from fixed-target experiments. Also shown is a NLO QCD fit⁴⁸ to the H1, NMC, and BCDMS data with $Q^2 > 5 \text{ GeV}^2$.

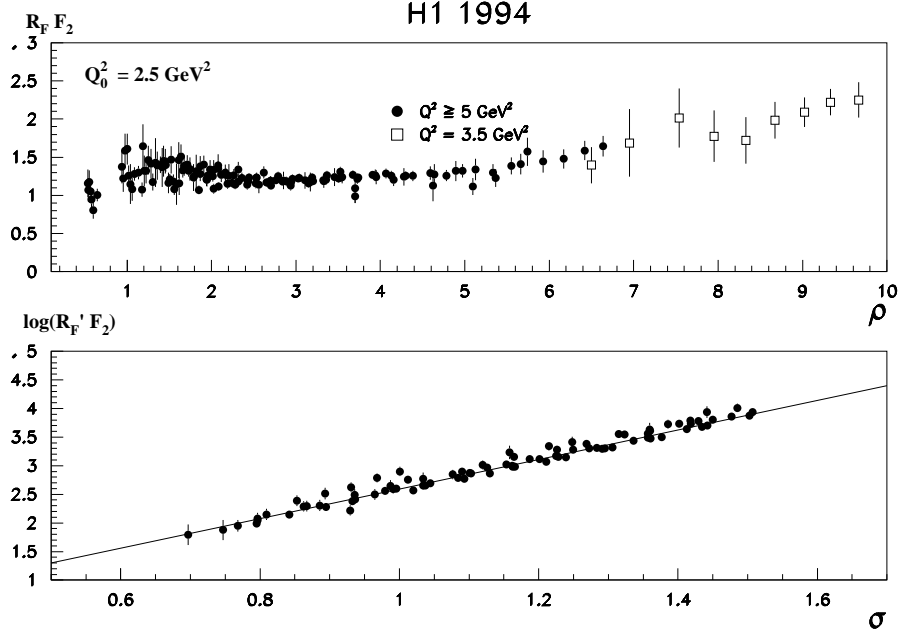


Figure 18: The rescaled structure function $R_F F_2$ as a function of ρ (top) and $\ln R'_F F_2$ as a function of σ^{48} (bottom).

parameter λ increases with Q^2 from about 0.2 at 10 GeV^2 to 0.3 at 100 GeV^2 and possibly to 0.5 at 1000 GeV^2 .⁴⁸ The rise of F_2 towards small x continues down to $Q^2 \simeq 1.5 \text{ GeV}^2$. Thus Regge-inspired models underestimate F_2 in this region. However, preliminary results from ZEUS⁷⁶ using the beam-pipe calorimeter and reaching down to $Q^2 = 0.16 \text{ GeV}^2$ and $x \simeq 3 \times 10^{-6}$ agree with the Donnachie–Landshoff model⁷⁷ below $Q^2 = 1 \text{ GeV}^2$.

The asymptotic behaviour of F_2 in the small- x -large- Q^2 range is generated by QCD dynamics^{78,79} and can be described by the two variables,

$$\sigma = \sqrt{\xi\zeta} \quad \text{and} \quad \rho = \sqrt{\xi/\zeta}, \quad (12)$$

with $\xi = \ln(x_0/x)$ and $\zeta = \ln \ln(Q^2/Q_0^2)$. In the HERA region $\ln F_2$ should grow linearly with σ and be independent of ρ . The σ slope can be calculated and one obtains $d \ln F_2 / d\sigma = 2\gamma = 2.5$ for five active flavours. With $R_F = R'_F \exp(-2\gamma)$ the quantity $R_F F_2$ becomes independent of both, σ and ρ . Here R'_F accounts for the finite size of σ and ρ . The HERA data impressively confirm this asymptotic behaviour as shown in Fig. 18. The σ slope of $\ln(R'_F F_2)$ fitted

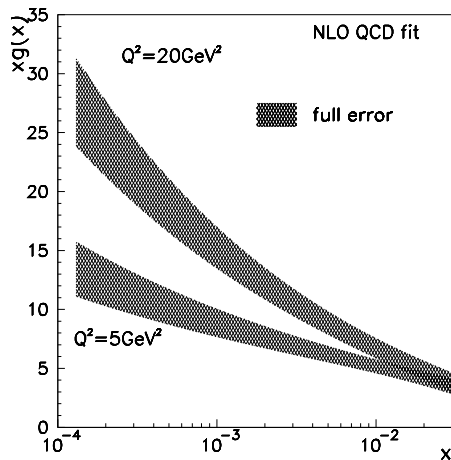


Figure 19: The NLO $\overline{\text{MS}}$ gluon distribution function, $xg(x)$, at $Q^2 = 5$ and 20 GeV^2 as a function of x from a QCD analysis of the H1 data.⁴⁸

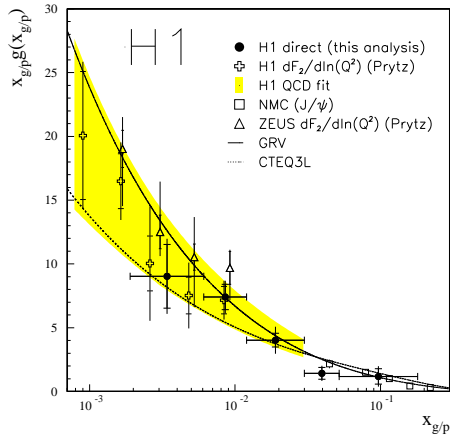


Figure 20: The leading-order gluon distribution function, $xg(x)$, at $Q^2 = 30 \text{ GeV}^2$ from (2+1)-jet data⁸¹ and from J/ψ production.⁸²

to the H1 data⁴⁸ is 2.57 ± 0.08 in good agreement with the prediction.

The strong correlation of the gluon distribution function with α_s at small x makes it difficult to determine α_s in a standard QCD analysis from the HERA F_2 data alone. However, the growth of F_2 in the small- x and large- Q^2 region is directly related to the value of α_s .⁷⁰ An analysis of the HERA data taken in 1993 yielded a rather high value compared to other DIS results, $\alpha_s(M_Z^2) = 0.120 \pm 0.005(\text{exp.}) \pm 0.009(\text{theory})$. A preliminary result from the 1994 data yields an even higher value of $0.122 \pm 0.004(\text{exp.})$.⁸⁰

The gluon distribution function determined in a next-to-leading order QCD analysis in the $\overline{\text{MS}}$ scheme from the H1 data⁴⁸ is shown in Fig. 19. New parton distribution functions from global fits including the new HERA data are available from the MRS⁸³ and CTEQ⁸⁴ groups. A direct measurement of $g(x)$ can be performed using the (2+1)-jet production data. From the photon-gluon fusion process, $\gamma^*g \rightarrow q\bar{q}$, two quark jets emerge. The target jet disappears in the beam pipe. There is an about 30 % contribution from the QCD Compton process, $\gamma^*q \rightarrow q' + g$. The (2+1)-jet production is via the photon-gluon fusion process directly linked to the gluon distribution in the proton. Leading-order results from the 1993 (2+1)-jet data from H1⁸¹ are shown in Fig. 20 together with NMC results from J/ψ production.⁸² They are in good agreement with other determinations of $xg(x)$.

7 Conclusions

The fixed-target structure function data are in good agreement. A small discrepancy in the small- x region persists between the muon and neutrino F_2 data. Presently, it is unclear whether this has a physics origin or is a reflection of experimental difficulties. This question is partly related to the rôle of strangeness in the nucleon and maybe also to the longitudinal structure function, F_L . For F_L considerable progress was made in the small- x region. However, it is still much less well known than F_2 . An accurate measurement at HERA, requiring a luminosity upgrade, is highly desirable. The theoretical understanding of higher-twist corrections, in particular of their x dependence, has made considerable progress over the last years and the calculations agree well with the data. This is an essential ingredient for the determination of α_s from sum rules, e.g. the Gross-Llewellyn Smith sum rule. While up to now most determinations of α_s from scaling violations in structure functions yielded consistently smaller results than obtained from LEP, the situation is less clear after the re-analysis of the CCFR structure functions. A determination of α_s from the small- x -high- Q^2 region of the HERA data yields also a rather large result. The rise of F_2 with decreasing x and increasing Q^2 has been mapped out at HERA with a considerable precision. Thus a good determination of the gluon distributions at small x became possible.

Deep inelastic scattering continues to be one of the most important testing grounds of perturbative – and to the extent our present understanding allows – also of nonperturbative QCD.

Acknowledgements

I thank my colleagues in the New Muon and Spin Muon Collaborations for many helpful discussions and B. Frois and V. W. Hughes for organising this stimulating Workshop in Erice and for their patience awaiting this manuscript.

- [1] X. Ji, J. Tang, and P. Hoodbhoy, *Phys. Rev. Lett.* **76** (1996) 740.
- [2] V. N. Gribov and L. N. Lipatov, *Sov. J. Nucl. Phys.* **15** (1972) 438;
L. N. Lipatov, *Sov. J. Nucl. Phys.* **20** (1975) 94.
- [3] Y. L. Dokshitzer, *Sov. Phys. JETP* **46** (1977) 461.
- [4] G. Altarelli and G. Parisi, *Nucl. Phys. B* **126** (1977) 298.
- [5] The CCFR Collaboration, A. O. Bazarko *et al.*, *Z. Phys. C* **65** (1995) 189.
- [6] The EM Collaboration, J. J. Aubert *et al.*, *Phys. Lett. B* **123** (1983) 275.
- [7] J. Ellis and R. L. Jaffe, *Phys. Rev. D* **9** (1974) 1444; *Phys. Rev. D* **10** (1974) 1669.
- [8] The EM Collaboration, J. Ashman *et al.*, *Phys. Lett. B* **206** (1988) 364.

- [9] The EM Collaboration, J. Ashman *et al.*, *Nucl. Phys. B* **328** (1989) 1.
- [10] The NM Collaboration, P. Amaudruz *et al.*, *Phys. Rev. Lett.* **66** (1991) 2712.
- [11] The NM Collaboration, M. Arneodo *et al.*, *Phys. Rev. D* **50** (1994) R1.
- [12] K. Gottfried, *Phys. Rev. Lett.* **18** (1967) 1154.
- [13] The H1 Collaboration, I. Abt *et al.*, *Nucl. Phys. B* **407** (1993) 515.
- [14] The ZEUS Collaboration, M. Derrick *et al.*, *Phys. Lett. B* **316** (1993) 412.
- [15] The H1 Collaboration, C. Adloff *et al.*, Preprint DESY 97-24 (Hamburg, Germany, February 1997), submitted to *Z. Phys. C*.
- [16] The ZEUS Collaboration, J. Breitweg *et al.*, Preprint DESY 97-25 (Hamburg, Germany, February 1997), submitted to *Z. Phys. C*.
- [17] R. D. Ball and A. de Roeck, in: Proceedings *Int. Workshop on Deep Inelastic Scattering and related Phenomena (DIS96)*, Roma, Italy, April 15–19, 1996, hep-ph/9609309.
- [18] The H1 Collaboration, S. Aid *et al.*, *Phys. Lett. B* **379** (1996) 319.
- [19] The ZEUS Collaboration, M. Derrick *et al.*, *Z. Phys. C* **72** (1996) 47.
- [20] C. G. Callan and D. J. Gross, *Phys. Rev. Lett.* **22** (1969) 156.
- [21] W. Zeuner, *these Proceedings*.
- [22] R. Taylor, *Rev. Mod. Phys.* **63** (1991) 573; H. Kendall, *Rev. Mod. Phys.* **63** (1991) 597; J. Friedman, *Rev. Mod. Phys.* **63** (1991) 615.
- [23] L. W. Whitlow, E. M. Riordan, and S. Dasu, *Phys. Lett. B* **282** (1992) 475.
- [24] T. Sloan, G. Smadja, and R. Voss, *Phys. Rep.* **162** (1988) 45.
- [25] The EM Collaboration, O. C. Allkofer *et al.*, *Nucl. Instrum. Methods* **179** (1981) 445.
- [26] The NM Collaboration, M. Arneodo *et al.*, submitted to *Nucl. Phys. B*, hep-ex/9611022.
- [27] The NM Collaboration, P. Amaudruz *et al.*, *Nucl. Phys. B* **441** (1995) 3.
- [28] The NM Collaboration, M. Arneodo *et al.*, *Nucl. Phys. B* **481** (1996) 23.
- [29] The E665 Collaboration, M. R. Adams *et al.*, *Phys. Rev. D* **54** (1996) 3006.
- [30] J. P. Berge *et al.*, *Z. Phys. C* **49** (1991) 187.
- [31] The CCFR Collaboration, W. C. Leung *et al.*, *Phys. Lett. B* **317** (1993) 655.
- [32] L. W. Whitlow *et al.*, *Phys. Lett. B* **250** (1990) 193.
- [33] G. Altarelli and G. Martinelli, *Phys. Lett. B* **76** (1978) 89.
- [34] The NM Collaboration, M. Arneodo *et al.*, *Nucl. Phys. B* **483** (1997) 3.
- [35] The CCFR/NuTeV Collaboration, A. Bodek *et al.*, *J. Phys. G* **22** (1996) 775.
- [36] NM, P. Amaudruz *et al.*, *Phys. Lett. B* **294** (1992) 120.
- [37] The E-140 Collaboration, S. Dasu *et al.*, *Phys. Rev. Lett.* **61** (1988) 1061
- [38] The E-140 Collaboration, S. Dasu *et al.*, *Phys. Rev. D* **49** (1994) 5641.
- [39] The E-140X Collaboration, L. H. Tao *et al.*, *Z. Phys. C* **70** (1996) 387.
- [40] The H1 Collaboration, C. Adloff *et al.*, Preprint DESY 96-236 (Hamburg, Germany, November 1996).
- [41] BCDMS, A. C. Benvenuti *et al.*, *Phys. Lett. B* **223** (1989) 485.
- [42] BCDMS, A. C. Benvenuti *et al.*, *Phys. Lett. B* **237** (1990) 592.
- [43] The EM Collaboration, J. J. Aubert *et al.*, *Nucl. Phys. B* **259** (1985) 189.
- [44] The EM Collaboration, J. J. Aubert *et al.*, *Nucl. Phys. B* **293** (1987) 740.

- [45] A. Milsztajn *et al.*, *Z. Phys. C* **49** (1991) 527.
- [46] K Bazizi and S. J. Wimpenny, Preprint UCR/DIS/91-02 (1991).
- [47] The NM Collaboration, M. Arneodo *et al.*, *Phys. Lett. B* **364** (1995) 107.
- [48] The H1 Collaboration, S. Aid *et al.*, *Nucl. Phys. B* **470** (1996) 3.
- [49] The ZEUS Collaboration, M. Derrick *et al.*, Preprint DESY 96-076 (Hamburg, Germany, 1996) submitted to *Z. Phys. C*.
- [50] The E665 Collaboration, M. R. Adams *et al.*, *Phys. Rev. Lett.* **75** (1995) 1466.
- [51] B. Badelek and J. Kwiecinski, *Nucl. Phys. B* **3270** (1992) 278; *Phys. Rev. D* **50** (1994) R4.
- [52] W. Melnitchouk and A. W. Thomas, *Phys. Rev. D* **47** (1993) 3783.
- [53] The NA51 Collaboration, A. Baldit *et al.*, *Phys. Lett. B* **332** (1994) 244.
- [54] The CCFR Collaboration, W. G. Seligman *et al.*, hep-ex/9701017.
- [55] The CCFR Collaboration, S. R. Mishra *et al.*, Preprint Nevis #1459 (June 1992).
- [56] The E-139 Collaboration, J. Gomez *et al.*, *Phys. Rev. D* **49** (1994) 4348.
- [57] The NM Collaboration, M. Arneodo *et al.*, *Nucl. Phys. B* **481** (1996) 3.
- [58] S. J. Brodsky, C. Peterson, and N. Sakai, *Phys. Rev. D* **23** (1981) 2745.
- [59] M. Burkhardt and B. J. Warr, *Phys. Rev. D* **45** (1992) 958.
- [60] V. Barone *et al.*, *Phys. Lett. B* **268** (1991) 279.
- [61] V. Barone *et al.*, *Phys. Lett. B* **304** (1993) 176.
- [62] A. Donnachie and P. V. Landshoff, *Z. Phys. C* **61** (1994) 139.
- [63] M. Virchaux and A. Milstajn, *Phys. Lett. B* **274** (1992) 221.
- [64] The NM Collaboration, P. Amaudruz *et al.*, *Nucl. Phys. B* **371** (1992) 3.
- [65] The NM Collaboration, M. Arneodo *et al.*, *Phys. Lett. B* **309** (1993) 222.
- [66] H. Georgi and H. D. Politzer, *Phys. Rev. D* **14** (1976) 1829; A. de Rújula, H. Georgi, and H. D. Politzer, *Ann. Phys.* **103** (1977) 315.
- [67] M. Dasgupta and B. R. Webber, *Phys. Lett. B* **382** (1996) 273.
- [68] The CCFR Collaboration, P. Z. Quintas *et al.*, *Phys. Rev. Lett.* **71** (1993) 1307.
- [69] The CCFR Collaboration, D. A. Harris *et al.*, in: J. Tran Thanh Van, ed., *Proceedings XXXth Rencontres de Moriond: QCD and High Energy Hadronic Interactions*, Meribel les Allues, France, 19–25 Mar 1995, (Editions Frontières, France, 1995) 247, hep-ex/9506010.
- [70] R. D. Ball and S. Forte, *Phys. Lett. B* **358** (1995) 365.
- [71] J. Chýla and L. A. Kataev, *Phys. Lett. B* **297** (1992) 385.
- [72] The Particle Data Group, R. M. Barnett *et al.*, *Phys. Rev. D* **50** (1994) 1.
- [73] D. J. Gross and C. H. Llewellyn Smith, *Nucl. Phys. B* **14** (1969) 337.
- [74] J. D. Bjorken, *Phys. Rev.* **148** (1966) 1467; *Phys. Rev. D* **1** (1970) 1376.
- [75] S. A. Larin and J. A. M. Vermaseren, *Phys. Lett. B* **259** (1991) 345.
- [76] The ZEUS Collaboration, Y. Zhu *et al.*, in: *Proceedings Int. Workshop on Deep Inelastic Scattering and related Phenomena (DIS96)*, Roma, Italy, April 15–19, 1996.
- [77] A. Donnachie and P. V. Landshoff, *Phys. Lett. B* **296** (1992) 227.

- [78] A. De Rújula *et al.*, *Phys. Rev. D* **10** (1974) 1649.
- [79] R. D. Ball and S. Forte, *Phys. Lett. B* **335** (1994) 77.
- [80] R. D. Ball and S. Forte, in: Proceedings *Int. Workshop on Deep Inelastic Scattering and related Phenomena (DIS96)*, Roma, Italy, April 15–19, 1996, hep-ph/9607289.
- [81] The H1 Collaboration, S. Aid *et al.*, *Nucl. Phys. B* **449** (1995) 3.
- [82] NM, D. Allasia *et al.*, *Phys. Lett. B* **258** (1991) 493.
- [83] A. D. Martin, R. G. Roberts, and W. J. Stirling, *Phys. Lett. B* **387** (1996) 419.
- [84] H. L. Lai *et al.*, *Phys. Rev. D* **55** (1997) 1280.